

# PHYSICAL REVIEW D

## PARTICLES AND FIELDS

THIRD SERIES, VOLUME 40, NUMBER 5

1 SEPTEMBER 1989

### Measurement of $\alpha_s$ from hadron jets in $e^+e^-$ annihilation at $\sqrt{s}$ of 29 GeV

W. T. Ford, N. Qi,<sup>(a)</sup> A. L. Read, Jr.,<sup>(b)</sup> and J. G. Smith  
*Department of Physics, University of Colorado, Boulder, Colorado 80309*

T. Camporesi,<sup>(c)</sup> R. De Sangro, I. Peruzzi, and M. Piccolo  
*Istituto Nazionale di Fisica Nucleare, Laboratori Nazionali di Frascati, Frascati, Italy*

R. B. Hurst,<sup>(c)</sup> J. Pyrlík, J. P. Venuti,<sup>(d)</sup> and R. Weinstein  
*Department of Physics, University of Houston, Houston, Texas 77004*

M. W. Gettner, G. P. Goderre,<sup>(e)</sup> J. C. Sleeman,<sup>(f)</sup> and E. von Goeler  
*Department of Physics, Northeastern University, Boston, Massachusetts 02115*

G. B. Chadwick, R. E. Leedy,<sup>(g)</sup> R. L. Messner, L. J. Moss, F. Muller,<sup>(h)</sup> H. N. Nelson,<sup>(c)</sup>  
D. M. Ritson, L. J. Rosenberg,<sup>(i)</sup> D. E. Wisner,<sup>(j)</sup> and R. W. Zdanko  
*Department of Physics, Stanford University, Stanford, California 94305*  
*and Stanford Linear Accelerator Center, Stanford University, Stanford, California 94309*

D. E. Groom<sup>(g)</sup> and P. G. Verdini<sup>(k)</sup>  
*Department of Physics, University of Utah, Salt Lake City, Utah 84112*

H. R. Band, M. C. Delfino,<sup>(l)</sup> J. R. Johnson, T. L. Lavine,<sup>(m)</sup> T. Maruyama, and R. Prepost  
*Department of Physics, University of Wisconsin, Madison, Wisconsin 53706*

(Received 17 February 1989)

A study of the lateral development of jets of hadrons produced in electron-positron annihilation has been used to determine the strong coupling constant  $\alpha_s$ . Data were obtained with the MAC detector at the SLAC  $e^+e^-$  storage ring PEP at  $\sqrt{s} = 29$  GeV. Based on the parton calculations of Gottschalk and Shatz, a value for  $\alpha_s$  of  $0.133 \pm 0.005(\text{stat}) \pm 0.009(\text{syst})$  has been determined for string fragmentation, and  $0.112 \pm 0.008(\text{stat}) \pm 0.007(\text{syst})$  for an independent-jet model.

#### I. INTRODUCTION

The theory of quantum chromodynamics (QCD) is believed to describe the strong interactions of hadrons. The running coupling constant  $\alpha_s$  is the fundamental parameter determining the strength of the strong interactions and a large number of experiments have been performed to determine its value. Measurements with  $e^+e^-$  colliders in the energy regime of PEP at SLAC and PETRA at DESY started with the observation of clear three-jet hadronic final states.<sup>1</sup> These measurements have yielded  $\alpha_s$  values ranging from 0.1 to 0.2 in the center-of-mass energy range 29–45 GeV. This range of values stems largely from the approximations inherent in the theories used to predict  $\alpha_s$ -sensitive observables.

The early measurements of  $\alpha_s$  were based on measurements of the fraction of three-jet events in the hadronic-

event samples (an example of a cluster method). This fraction, to lowest order, is proportional to  $\alpha_s$ :

$$\sigma_{3\text{-jet}}/\sigma_{\text{hadrons}} = k\alpha_s, \quad (1)$$

where  $k$  can be predicted from perturbative QCD with appropriate resolution cuts to separate three-jet events from two-jet events at the parton level. The predictions for soft fragmentation of quarks and gluons into hadrons is obtained from various phenomenologically motivated models. The algorithm for defining jets is highly model dependent and produced large corrections to  $k$ . This provided the motivation to find experimental observables that were sensitive to  $\alpha_s$ , yet independent of details of the soft fragmentation.

One of the methods on which attention centered was based on the energy-energy correlation as the observable.<sup>2</sup> The measurements are based on the quantity

$$\frac{1}{\sigma_0} \frac{d\Sigma}{d \cos\chi} = \frac{1}{N \Delta \cos\chi} \sum_i \sum_j \frac{E_i E_j}{s}, \quad (2)$$

where  $N$  is the number of events, and  $\chi$  is the angle between calorimeter cells in an event recording energy  $E_i$  and  $E_j$ . The contribution from the region near  $\chi=90^\circ$ , away from two-jet fragmentation, will be sensitive to  $\alpha_s$ . The energy-energy correlation asymmetry (EECA)

$$A(\chi) = \frac{1}{\sigma_0} \left[ \frac{d\Sigma}{d \cos\chi}(\pi - \chi) - \frac{d\Sigma}{d \cos\chi}(\chi) \right] \quad (3)$$

is used to measure  $\alpha_s$ . In principle this method requires no detailed event reconstruction and it was expected that the EECA would be independent of the fragmentation model assumptions. Previous MAC results<sup>3</sup> and other studies<sup>4</sup> found substantial model dependence, and measurements based on the EECA typically restrict fits to the central region in order to minimize its influence.

An alternative method exploits the fact that radiative QCD processes enhance the jet  $p_\perp$  distribution at large values of  $p_\perp$  relative to the jet axis (an example of a shape method). For large enough values of  $p_\perp$ , the integral spectrum of the  $p_\perp$  distribution is proportional to  $\alpha_s$ :

$$\sigma_{\text{large}} / \sigma_{\text{hadrons}} = k \alpha_s, \quad (4)$$

where this  $k$  is again calculable from perturbative QCD. In the method detailed below, calorimeter energy vectors are used in place of momentum vectors, and we sum the absolute  $E_\perp$  values for the widest ("fat") jet in an event and use the distribution of the summed  $E_\perp$ 's as a measure of  $\alpha_s$ . The method is direct and requires only calorimetric information. It will be shown that this observable is highly sensitive to  $\alpha_s$  though it exhibits model dependence.

The question as to which observable provides the best measure of  $\alpha_s$  is complicated. It is desirable that a selected observable have only minimal dependence on details of soft fragmentation. In other words, the power-law corrections arising from fragmentation should fall off as rapidly as possible. When rather naive soft fragmentation is considered, as occurs in models with massless quarks that fragment independently, the EECA picks up order- $(1/Q)^2$  corrections,<sup>2</sup> where  $Q^2$  is the characteristic off-shell parton mass, while most shape and cluster measures pick up order  $1/Q$  corrections.<sup>5</sup> Adding quark masses to the EECA perturbative predictions introduces  $1/Q$  corrections,<sup>6</sup> as do the correlations associated with strings or boosts.<sup>7</sup> Hence, realistic assumptions result in  $1/Q$  corrections for all the above observables and, in particular, the EECA has a stronger dependence on fragmentation than originally thought.

Given the lack of a firm theoretical prejudice as to what would be the best observable, we have taken an empirical approach. We conducted a Monte Carlo study of likely shape, cluster, and EECA observables, seeking ones that vary the least when the fragmentation model is changed. We find that those observables related to the jet  $p_\perp$  are least dependent upon the choice of fragmentation models while exhibiting the desired sensitivity to  $O(\alpha_s)$

effects. The actual variable chosen is the momentum transverse to the overall jet axis of the event, projected into the event plane. This quantity is strongly correlated to the directions of the hardest partons. Since the "thin" jet fragmentation is dominated by nonperturbative effects, we increase sensitivity to perturbative effects by including particles from the fat jet in an event, which yields a quantity we call  $P_{1>}^{\text{in}}$ . This observable is related to sphericity,<sup>8</sup> the properties of which have been studied in detail.<sup>5</sup> We use the calorimetry of MAC to measure the energy equivalent quantity  $E_{1>}^{\text{in}}$ . Other authors<sup>9</sup> have observed that quantities related to  $P_{1>}^{\text{in}}$  can be particularly insensitive to the choice of fragmentation models. The sensitivity of several shape, cluster, and EECA measures of  $\alpha_s$  to different fragmentation schemes has been compared in a theoretical study,<sup>10</sup> with the result that the EECA fares poorly in comparison to some shape measures even for rather large  $\sqrt{s}$ .

Most of the recent  $\alpha_s$  measurements from PEP and PETRA experiments have concentrated on the EECA as the  $\alpha_s$ -sensitive observable, with use of one particular perturbative calculation<sup>11</sup> of the  $O(\alpha_s^2) e^+e^- \rightarrow$  quarks + gluons. Owing to the nature and implementation of this  $O(\alpha_s^2)$  calculation in a Monte Carlo program, verification and comparison with similar energy-energy correlation asymmetry studies is difficult. QCD, unlike QED which has a coupling constant an order of magnitude smaller, requires that perturbative calculations carefully treat contributions from higher-order terms. There now exist calculations that have carefully reconsidered these higher-order contributions.<sup>12</sup> Thus we present a measurement of  $\alpha_s$  that features jet  $E_{1>}^{\text{in}}$  as the  $\alpha_s$ -sensitive observable, with perturbative QCD predictions from a recent, complete (with one exception discussed later) and robust  $O(\alpha_s^2)$  calculation of  $e^+e^- \rightarrow$  quarks + gluons.

## II. EXPERIMENTAL TECHNIQUE

This analysis uses approximately  $220 \text{ pb}^{-1}$  of  $e^+e^-$  annihilation data accumulated at  $\sqrt{s}=29 \text{ GeV}$ . This integrated luminosity yielded approximately  $10^5$  multihadron events.

### A. Apparatus

The MAC detector has been described in detail elsewhere.<sup>13,14</sup> The solid angle instrumented in MAC is about 98% of  $4\pi$  sr. This almost complete coverage is ideal for calorimetric jet studies since observables such as thrust are reconstructed with little distortion by the apparatus. Since this analysis heavily relies upon the MAC calorimetry, we briefly discuss the construction and performance of the calorimetry systems.

Figure 1 shows end and side views of the MAC detector. The following discussion concentrates on the central barrel electromagnetic-shower chambers and hadron calorimeters.

### B. Electromagnetic shower chambers

The hexagonally symmetric shower-chamber (SC) system provides full azimuthal coverage. Each sextant is

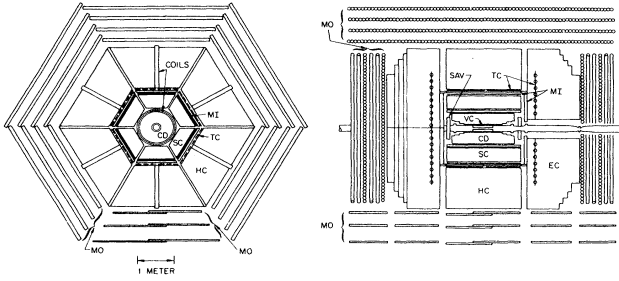


FIG. 1. End and side views of the MAC detector.

composed of 32 2.5-mm-thick lead plates interleaved with proportional wire chambers (PWC's). Sense wires traverse the length of a grounded aluminum extrusion, each extrusion containing eight adjacent cells with dimensions 1.8 cm wide by 0.86 cm high. The segmentation of the SC is illustrated in Figs. 2(a) and 2(b). The wires in each sextant are grouped into 32 azimuthal wedges. Each wedge is further divided into three radial layers, called wire groups; in order of increasing radius, the layers are composed of 7, 13, and 12 wire planes. The outputs of low input-impedance preamplifiers at each end

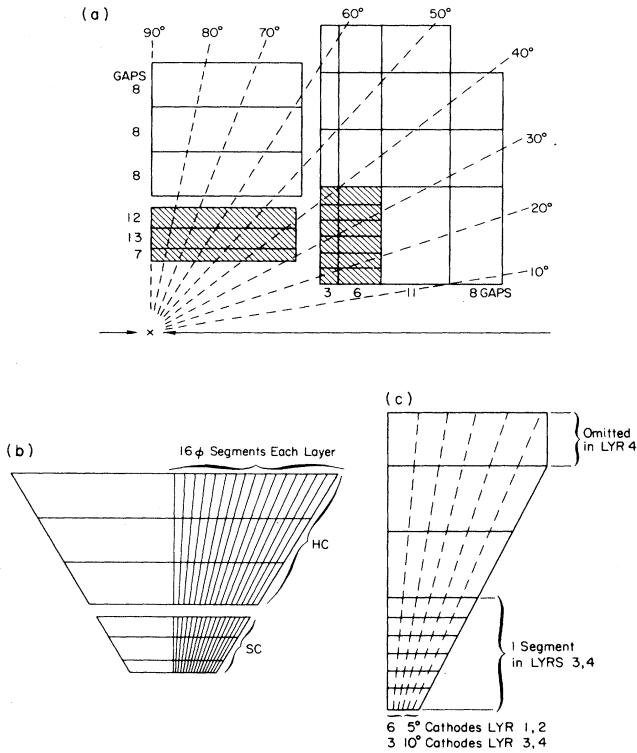


FIG. 2. Segmentation of the various calorimeters. (a) Side view of the calorimetry. The electromagnetic shower systems are shown shaded. The number of wire planes in each radial layer is also indicated. (b) View along the beam line of the central section calorimetry. Each sextant of the SC and HC is divided into 32 azimuthal wedges of anode wires. These are further subdivided into three radial layers. (c) View along the beam line of the end-cap calorimetry.

of each wire group are connected to analog sample-and-hold modules (SHAM's)<sup>15</sup> which are, in turn, read out by an analog-to-digital scanner module (BADC).<sup>16</sup> Fast analog sums are used for the hardware and software triggers. The dynamic range of the electronics is such that minimum-ionizing tracks and heavily-ionizing showers are both within the digitization range. The z-coordinate information of a shower comes from current division, which results in an energy vector  $\mathbf{E}$  for each wire group. The solenoid coil together with the SC total approximately 14 radiation lengths for electrons at normal incidence.

The gas used is 85% argon with 15% methane. A separate small proportional chamber monitors the gain of the recirculated gas at the exhaust port with the 6-keV x-ray line of  $\text{Fe}^{55}$ , relative to the gain of a fiducial gas mixture. A better correction is later achieved by using the SC response in Bhabha-scattering events.

### C. Hadron calorimeter

The central-section hadron calorimeter (HC) is composed of six separate stacks of steel sandwiched with PWC planes. Each sextant stack is composed of 24 2.5-cm-thick steel plates followed by three additional 10-cm-thick steel plates, providing a total of 4.3 nuclear interaction lengths through the HC steel for pions at normal incidence. Each extrusion is about 230 cm long, 20 cm wide, and 1.5 cm high, and encloses eight side-by-side cells. The first three steel plates in each sextant provide flux return for the solenoid field. The remaining steel in each HC sextant is surrounded by a water-cooled four-turn aluminum coil producing a toroidal field of about 17.5 kG.

The segmentation of the end-cap calorimetry is shown in Fig. 2(c). The segmentation of the HC wires into wire groups is similar to the SC segmentation. Each HC sextant has 32 azimuthal wedges subdivided into three layers of eight PWC planes per layer, resulting in 96 wire groups. The first two layers have outputs at both ends to allow for current division. The third layer is single ended. There is one PWC plane in each of the two gaps be-

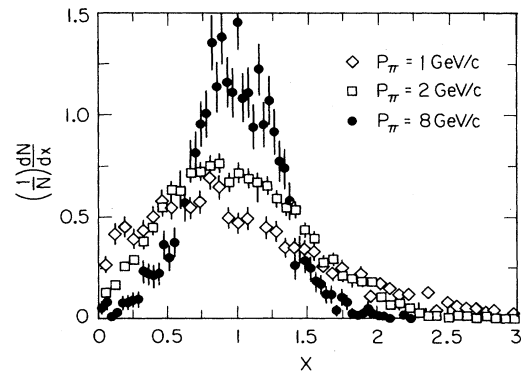


FIG. 3. Resolution of a prototype HC assembly for a variety of incident pion momenta. The quantity  $X$  is the ratio of measured energy deposition to incident pion momentum. All momenta are consistent with a resolution of  $\Delta E/E \sim 75\%/\sqrt{E}$  (GeV).

tween the 10-cm-thick steel plates; these are for muon tagging and are not used in the HC energy sums.

The gas gain in the HC is monitored as described above for the SC and is also checked with data from cosmic rays. A prototype HC assembly was placed in a test beam<sup>17</sup> and the energy resolution measured for various incident pion momenta. The measured resolutions shown in Fig. 3 are consistent with a resolution of  $\Delta E/E \sim 75\%/\sqrt{E}$  (GeV).

#### D. Definitions of experimental quantities

The thrust axis of an event<sup>18</sup> is determined by maximizing, with respect to direction  $\hat{n}$ , the quantity

$$T = \frac{\max_{|\hat{n}|=1} \sum_i |\hat{n} \cdot \mathbf{E}_i|}{E_{\text{vis}}}, \quad (5)$$

with  $i$  the index of each calorimeter hit, and  $E_{\text{vis}} = \sum_i |\mathbf{E}_i|$ . Note that here calorimetric vectors replace momentum vectors used in the original definition. The resultant maximal  $T$  is the thrust value and the corresponding  $\hat{n}$  is the thrust-axis direction  $\hat{\mathbf{T}}$ . Single-ended calorimeter hits, which are omitted from the sum because their  $z$  component is not measured, typically account for less than 1 GeV of the visible energy deposition.

A repeat of the thrust calculation, with the added constraint that  $\hat{n} \cdot \hat{\mathbf{T}} = 0$ , yields the quantities  $T_{\text{maj}}$  and  $\hat{\mathbf{T}}_{\text{maj}}$ , the value and direction of the major axis. The minor axis is defined by  $\hat{\mathbf{T}}_{\text{min}} \equiv \hat{\mathbf{T}} \times \hat{\mathbf{T}}_{\text{maj}}$ . The magnitude of  $\hat{\mathbf{T}}_{\text{min}}$  is similarly defined as

$$T_{\text{min}} = \frac{\sum_i |\hat{\mathbf{T}}_{\text{min}} \cdot \mathbf{E}_i|}{E_{\text{vis}}}. \quad (6)$$

These thrust-related axes have an approximate physical interpretation when applied to partons in a three-jet event. Here  $\hat{\mathbf{T}}$  is collinear with the most energetic of the primary partons,  $\hat{\mathbf{T}}_{\text{maj}}$  and  $\hat{\mathbf{T}}$  together define the parton event plane, and  $\hat{\mathbf{T}}_{\text{min}}$  is normal to the parton event plane.

The nearly hermetic calorimetric coverage of the MAC detector allows accurate reconstruction of the thrust

direction. The distribution of the difference in angle between the thrust direction before and after Monte Carlo simulation of the detector is shown in Fig. 4. The thrust direction is typically determined with an accuracy of better than 5°.

We define the hemispheric energy-flow moments

$$E_{\pm}^{\text{in}} \equiv \sum_i |\mathbf{E}_i \cdot \hat{\mathbf{T}}_{\text{maj}}| \theta(\pm \mathbf{E}_i \cdot \hat{\mathbf{T}}), \quad (7)$$

where the  $\theta$  function in  $E_{\pm}^{\text{in}}$  ( $E_{\pm}^{\text{in}}$ ) has contributions from calorimeter hits in the same (opposite) hemisphere as the thrust axis. Finally, we define the quantity

$$E_{\pm}^{\text{in}} = \max\{E_{\pm}^{\text{in}}, E_{\pm}^{\text{in}}\}, \quad (8)$$

which is the  $\alpha_3$ -sensitive observable used in this study.

#### E. Hadron filter

Hadronic events are selected with the hadron filter, a set of cuts to select events arising from one photon annihilation into hadrons, over a broad range of particle multiplicities and production angles. The details of the hadron filter have been published previously.<sup>14</sup> The hadron filter has an acceptance of about 78% of the total hadronic cross section and allows only about 3% contamination, mostly from  $2\gamma$  (2%) and  $\tau^+\tau^-$  events (1%). The hadron filter selected 100 475 events from the 220-pb<sup>-1</sup> sample.

#### F. Central filter

The detector response, owing to the barrel-like segmentation and construction of the apparatus, is very uniform in  $\phi$ , and slightly less so in  $\theta$ . The central calorimeters cover the approximate angular range  $60^\circ < \theta < 120^\circ$  away from the beam [see Fig. 2(a)]. The region  $30^\circ < \theta < 60^\circ$  and  $120^\circ < \theta < 150^\circ$  is a transition region between the central and end-cap calorimeters and is responsible for some variation in calorimeter response. More importantly, for thrust angles in the range  $\theta < 30^\circ$  and  $\theta > 150^\circ$ , energy is likely to be lost along the direction of the beam pipe, thus distorting the reconstructed thrust direction.

Our analysis requires unbiased reconstruction of thrust direction and event-plane orientation. The most uniform calorimeter response, with the smallest energy leakage, is achieved within the MAC central barrel calorimeters. The central filter is therefore designed to select hadronic events with thrust directions constrained to the central region, and event planes nearly perpendicular to the beam direction.

##### 1. Cuts for the central filter

In terms of the quantities

$$\theta_{\text{thrust}} \equiv \theta \text{ of the thrust axis,}$$

$$E_{\text{vis}} \equiv \sum_i |\mathbf{E}_i|,$$

$i$  runs over all two-ended calorimeter hits,

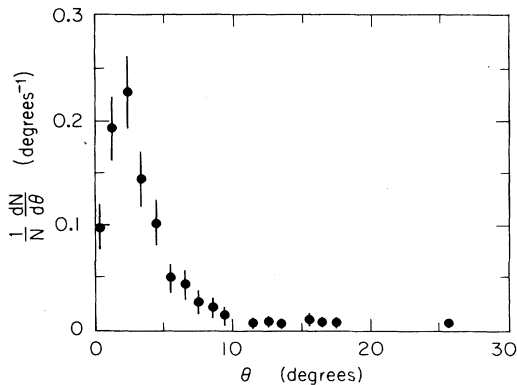


FIG. 4. Angular difference in thrust direction before and after Monte Carlo simulation of the detector response.

$$E_{EC} \equiv \sum_i |\mathbf{E}_i| ,$$

$i$  runs over all hits in the end-cap calorimeters ,

$$E_{CC} \equiv \sum_i |\mathbf{E}_i| ,$$

$i$  runs over all hits in the central calorimeters ,

the central filter cuts are given by

$$60^\circ < \theta_{\text{thrust}} < 120^\circ ,$$

$$E_{EC}/E_{CC} < 0.25 ,$$

$$24 \text{ GeV} < E_{\text{vis}} < 34 \text{ GeV} .$$

The thrust direction cut selects events depositing energy primarily in the central calorimeters. The cut on  $E_{EC}/E_{CC}$  further constrains energy deposition to be in the central calorimeters and also favors events with the event plane oriented perpendicular to the beam direction, so that the event plane is largely contained within the central calorimeters. The  $E_{\text{vis}}$  cut minimizes large gain fluctuations and cuts out  $2\gamma$  contamination. Figure 5 shows the relevant distributions and indicates the placement of the various cuts.

## 2. Acceptance

The cuts on  $\theta_{\text{thrust}}$ ,  $E_{EC}/E_{CC}$ , and  $E_{\text{vis}}$  each pass separately about 50% of the events. Overall, about 21% of the events selected by the hadron filter pass the central filter, yielding 21 061 events.

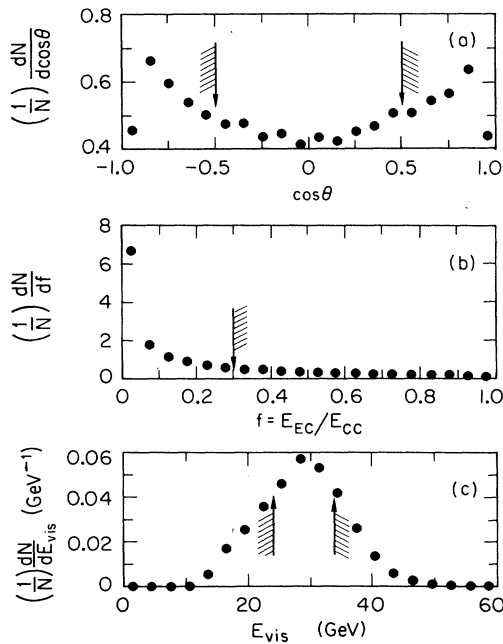


FIG. 5. Location of cuts in the central filter as shown for the data: (a)  $\theta_{\text{thrust}}$  determined with calorimetry, (b) end-cap energy divided by central-section energy, and (c) total calorimeter energy.

## III. EXTRACTION OF $\alpha_s$ FROM THE DATA

We use a Monte Carlo method to compute the distribution of observables as functions of  $\alpha_s$  and other model parameters. Here we discuss the QCD and fragmentation calculations entering into these computations.

### A. Perturbative QCD predictions

The total cross section for the process  $e^+e^- \rightarrow$  quarks + gluons to  $O(\alpha_s^2)$  may be written as

$$\sigma_{\text{tot}} = \sigma_{2\text{-parton}} + \sigma_{3\text{-parton}} + \sigma_{4\text{-parton}} . \quad (9)$$

The bare parton contributions contain divergences. The required finite  $\sigma_{\text{tot}}$  is a result of introducing a resolution criterion that allows the individually divergent bare parton terms to combine into finite dressed terms. Equation (9) then becomes

$$\sigma_{\text{tot}} = \sigma_{2\text{-jet}} + \sigma_{3\text{-jet}} + \sigma_{4\text{-jet}} . \quad (10)$$

The  $O(\alpha_s^2)$   $\sigma_{4\text{-jet}}$  term contains straightforward tree diagrams.<sup>19</sup> The  $\sigma_{2\text{-jet}}$  term is rather complicated since it contains loops and higher-order contributions, but is deduced by subtraction given  $\sigma_{3\text{-jet}}$ , since  $\sigma_{4\text{-jet}}$  and  $\sigma_{\text{tot}}$  are known.<sup>20</sup>

The dressed three-jet cross section  $\sigma_{3\text{-jet}}$  has been estimated by several authors. The  $\sigma_{3\text{-jet}}$  calculation of Fabricius, Kramer, Schierholz, and Schmitt<sup>21</sup> (FKSS) contains approximations that have been shown<sup>22</sup> to lead to overestimates of  $\alpha_s$  in fits to data. The improved calculation of Kunszt<sup>11</sup> and Ellis, Ross, and Terrano<sup>19</sup> (ERT) has been used for several more recent experimental analyses. The recent calculation of Gottschalk and Shatz<sup>12</sup> (GS) is more complete and represents an advance over earlier work, as discussed below.

The FKSS calculation, used in the Lund Monte Carlo FORTRAN code,<sup>23</sup> results in  $\alpha_s$  values of about 0.17 for fits to string fragmentation, and  $\alpha_s$  values of about 0.13 from fits to independent jet fragmentation. (These observations are made more precise in Sec. IV.) However, as previously mentioned, the FKSS calculation is approximate; some of the resolution-dependent terms are omitted, and these can be large in certain regions of phase space. The ERT calculation, first used by the Mark J Collaboration<sup>24</sup> to measure  $\alpha_s$ , retains all jet-resolution-dependent terms, at the expense of a very inefficient Monte Carlo numerical integration. The procedure is inherently difficult to invert, so observables corrected for QED and detector effects are difficult to extract for comparison with other experiments that also used EECA. The GS calculation retains the resolution-dependent terms and the analytic calculation allows for highly efficient event generation. The parton generation is easy to implement in the Monte Carlo framework.

Since both the ERT and GS calculations incorporate all the jet-resolution terms missing from the FKSS calculation, identical results might be expected. This is not the case; observable perturbative quantities differ. As an example, we examine the thrust distribution of partons generated by each of the calculations. We expect that the fraction of events with small values of thrust, being an in-

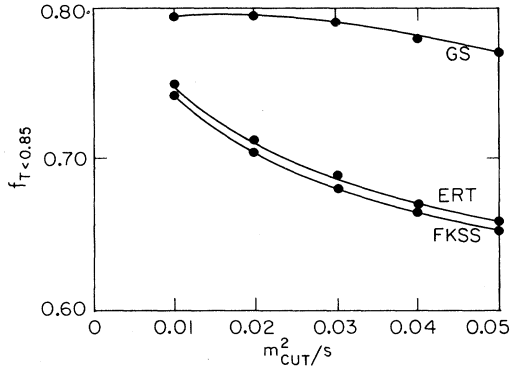


FIG. 6. Fraction of events with thrust less than 0.85 vs IR mass cut for the FKSS, ERT, and GS calculations. The typical statistical error is 0.01 per point.

frared stable observable, should be insensitive to the precise value of the jet-resolution cut in the calculations. Figure 6 shows, for  $\alpha_s = 0.13$ , the fraction of parton configurations with thrust less than 0.85 as a function of the value of the minimum scaled mass between any two partons,  $m_{ij}^2/s$  (the jet-resolution parameter used hereafter). The FKSS and ERT calculations predict a rather strong cutoff dependence,<sup>25</sup> while the GS prediction varies relatively little.

The difference between the GS and ERT calculations might be due to the different methods of applying jet-resolution cuts.<sup>26</sup> The ERT method seems to underpopulate certain regions of phase space. For example, configurations with low-mass quark pairs are excised even though these contributions are nonsingular and should remain. This approximate phase-space treatment results in effects dependent on the precise value of the resolution cut used. The GS calculation, being complete in this regard, is more stable with respect to changes of the resolution cut value.

Thus, with the exception of the treatment of quark masses (discussed below), the GS calculation represents the first complete and efficient parton generation for  $e^+e^- \rightarrow \text{quarks} + \text{gluons}$  to  $O(\alpha_s^2)$ . In the remainder of this paper, we present fits of  $\alpha_s$  with the GS calculation and compare with the results of the FKSS calculation.

### 1. The problem of quark masses

The  $O(\alpha_s^2)$  calculations discussed earlier generate the parton cross sections with the assumption of massless quarks. This limitation was not considered very serious, as it had been shown that, at least in the case of the energy-energy correlation asymmetry, the three- and four-jet Born terms are only slightly modified (at about the 10% level; Ref. 6) by mass corrections. Chosen for study because they are the easiest to calculate, these terms are the only ones that have no contribution from low-mass parton pairs after resolution cuts. It is unknown whether the mass effects will remain small for a complete calculation that must include finite terms remaining from the delicate cancellations of divergent diagrams.

However, some means must be made for incorporating heavy quarks since their decays can have a considerable effect on fits to  $\alpha_s$ . We have modified the calculation in an *ad hoc* way in order to include quark masses. For two-jet final states, masses were simply inserted with an appropriate energy rescaling. For three-jet final states, the  $O(\alpha_s)$  cross section of Ioffe<sup>27</sup> was used. The four-jet cross section was modified with the cuts described by Sjöstrand for the Lund Monte Carlo program.<sup>28</sup> We found that failure to model the effects of heavy quarks and their subsequent decays results in values of  $\alpha_s$  larger by as much as 25%.

## B. Fragmentation models

We model the evolution of the colored partons of perturbative QCD into colorless hadrons with phenomenological Monte Carlo programs. There is extensive literature for these models,<sup>29</sup> and we review it here briefly. We consider those fragmentation models falling into two classes: string models and independent jet models. The string models feature color strings stretched between color charges. The strings break to produce hadrons. Energy and momentum are conserved throughout the evolution. Independent jet models have quarks and gluons fragmenting independently of each other. Energy and momentum conservation is imposed *a posteriori*. One method is to boost the hadron center of mass to the laboratory frame, then rescale the event energy (the Ali or boost method). Another way is to fix the jet directions and rescale the longitudinal jet momenta (the Hoyer method). The fact that the various fragmentation models yield different final states is the major source of systematic uncertainty in this study.

## C. The dependence of $E_{1>}^{\text{in}}$ on $\alpha_s$ and fragmentation parameters

We wish to use  $E_{1>}^{\text{in}}$ , defined in Eq. (8), as the  $\alpha_s$ -sensitive observable. Our expectation is that gluon emission will manifest itself in fragmentation with a larger jet  $E_{1>}$  so the fat side of the hadronic event is a more accu-

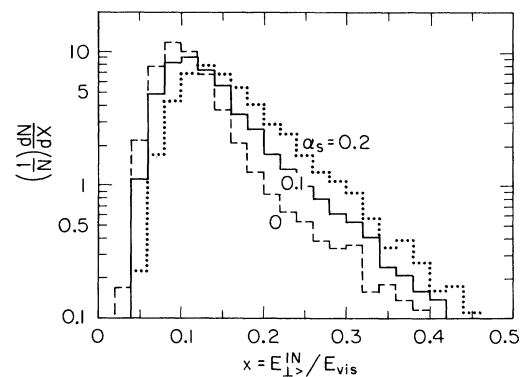


FIG. 7. Variation of  $E_{1>}^{\text{in}}/E_{\text{vis}}$  distribution with  $\alpha_s$ . The three histograms shown are for a string model with  $\alpha_s$  of 0, 0.1, and 0.2.

rate probe of the perturbative QCD process, while the thin side will be dominated by soft fragmentation. In addition, by projecting the energies onto the event plane, we enhance the contribution of single-gluon emission relative to multiple parton emission (which is not accounted for in the QCD calculation). We now determine how closely  $E_{1>}^{\text{in}}$  approaches an ideal observable.

### 1. Sensitivity to $\alpha_s$

As expected,  $E_{1>}^{\text{in}}$  is sensitive to variations in  $\alpha_s$ . This is shown in Fig. 7 for Monte Carlo events satisfying the central filter at  $\alpha_s$  of 0, 0.1, and 0.2, where the string model was used for the fragmentation. Observe that the integrated tail of the distribution is approximately linearly dependent upon  $\alpha_s$ . For this and the following three figures, nominal values of the fragmentation parameters are  $\alpha_s=0.18$ ,  $\sigma_q=0.311$  GeV/c, and  $\epsilon_c=0.250$  ( $Z_c^{\text{max}}\simeq 0.6$ ), with FKSS matrix elements applied to string fragmentation.

### 2. Sensitivity to $\sigma_q$

We expect the transverse-energy structure of hadronic events to depend on  $\sigma_q$ , the width of the secondary quark  $p_{\perp}$  distribution relative to the primary parton direction for the independent-jet models, or to the axis of the string in the string rest frame in the case of the string model. The dependence of  $E_{1>}^{\text{in}}$  upon  $\sigma_q$  is shown in Fig. 8 for string fragmentation and for the rather extreme range of  $\sigma_q$  represented by 212, 311, and 424 MeV/c. This effect, though not as great as seen by variation of  $\alpha_s$ , is still non-negligible, even at the extreme of the distribution.

### 3. Sensitivity to remaining parameters

The remaining fragmentation parameters have substantially less effect on the  $E_{1>}^{\text{in}}$  distribution, especially at the high- $E_{\perp}$  end. These other fragmentation parameters are discussed in decreasing order of importance.

The jet-resolution cut used in the FKSS QCD matrix elements can have an effect on the  $E_{1>}^{\text{in}}$  distribution. The

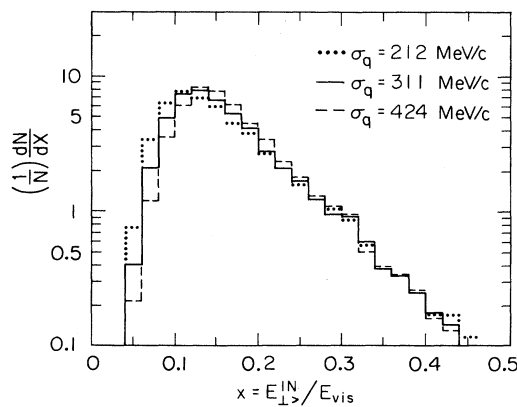


FIG. 8. Variation of  $E_{1>}^{\text{in}}/E_{\text{vis}}$  distribution with  $\sigma_q$ . The three curves shown are for a string model with a wide range of  $\sigma_q$  values represented by 212, 311, and 424 MeV/c.

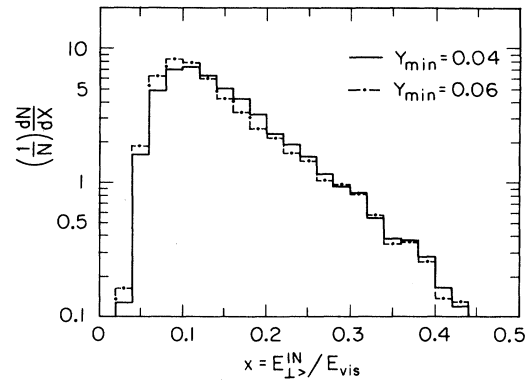


FIG. 9. Variation of  $E_{1>}^{\text{in}}/E_{\text{vis}}$  distribution with  $Y_{\text{min}}$ , according to the FKSS calculation. The two curves shown are for a string model with two widely separated values of  $Y_{\text{min}}$  of 0.04 and 0.06. The GS calculation introduces even less cutoff dependence.

cut used in an invariant-mass cut between any two partons in the event. Specifically, the type of cut studied in detail here requires  $Y_{ij} > Y_{\text{min}}$ , where  $Y_{ij} = m_{ij}^2/s$  is the square of the scaled invariant mass between partons  $i$  and  $j$ . As  $Y_{\text{min}}$  increases, the number of three- and four-jet events decreases, though the hard, wide-angle radiative component is largely unaffected. This tends to decrease the population in the high- $E_{\perp}$  end of the normalized  $E_{1>}^{\text{in}}/E_{\text{vis}}$  distribution. In practice,  $Y_{\text{min}}$  is set as small as possible; the lower limit of  $Y_{\text{min}}$  is reached when unphysical values for the QCD matrix elements result. The dependence of  $E_{1>}^{\text{in}}$  on the QCD jet-resolution cut is shown in Fig. 9. It should be noted that  $E_{1>}^{\text{in}}$  is only weakly dependent on  $Y_{\text{min}}$ , with decreasing sensitivity towards the high  $E_{\perp}$  end of the distribution; the crossover point is somewhere below  $E_{1>}^{\text{in}}/E_{\text{vis}}=0.2$ . The GS calculation also uses jet resolution cuts, but is significantly less sensitive than FKSS to this variation.

The shape of the fragmentation functions has a slight effect on the population at the large  $E_{\perp}$  end of the  $E_{1>}^{\text{in}}$  distribution. As an example of this dependence, we show in Fig. 10 the effect of changing the peak of the Peter-

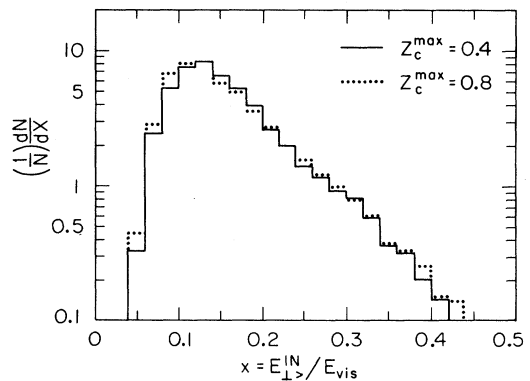


FIG. 10. Variation of  $E_{1>}^{\text{in}}/E_{\text{vis}}$  distribution with  $Z_c^{\text{max}}$ , the peak of the charmed-quark fragmentation function. The two curves shown use the Peterson form for the charmed-quark fragmentation function with two extreme  $Z_c^{\text{max}}$  values of 0.4 and 0.8.

son<sup>30</sup> form of the charmed-quark fragmentation function  $Z_c^{\max}$ , from 0.4 to 0.8. The  $Z_c^{\max}$  values of 0.4 (0.8) correspond to  $\epsilon_c$  of 0.9 (0.05). This represents an extreme range of values for the charmed-quark fragmentation function,<sup>31</sup> yet the effect on the  $E_{1>}^{\text{in}}$  distribution is slight and decreases at the high- $E_1$  end. The experimental uncertainty in the bottom-quark fragmentation function is greater, though the suppression of production of bottom quarks relative to charmed quarks makes the smaller uncertainty in the charmed-quark fragmentation more significant. The uncertainty in the  $a$  parameter of the Field and Feynman fragmentation functions<sup>32</sup> for the lighter quarks is considerably less.<sup>33</sup>

Other parameters of the soft fragmentation have been varied in a similar manner to determine their effect on the  $E_{1>}^{\text{in}}$  distribution. Only two of these parameters appears to have even a slight effect on the  $E_{1>}^{\text{in}}$  distribution. These parameters are  $P/V$ , the ratio of pseudoscalar to vector mesons produced in the fragmentation, and  $P(qq)/P(q)$ , the ratio of diquark pairs to quark pairs produced in the fragmentation (this regulates baryon production in the string and independent-jet models that we used). The remaining parameters had no statistically significant effect on the  $E_{1>}^{\text{in}}$  distribution.

#### D. The fit procedure

The fit procedure consists of two parts: constructing an analytic expression representing the bin contents of the  $E_{1>}^{\text{in}}$  distribution as a function of  $\alpha_s$  and  $\sigma_q$ , and varying  $\alpha_s$  and  $\sigma_q$  to obtain good agreement between the data and the analytic expression.

#### 1. Construction of the analytic form of $E_{1>}^{\text{in}}$

The objective is to construct an analytic expression for the contents of the  $i$ th bin of  $E_{1>}^{\text{in}}$  as a function of  $\alpha_s$  and  $\sigma_q$ . Ideally, at each value of  $\alpha_s$  and  $\sigma_q$  required in the fitting procedure, a complete Monte Carlo prediction of  $E_{1>}^{\text{in}}$  should be made. However, these Monte Carlo predictions are computer intensive, taking about 5 sec/event (on an IBM 3081K), making this direct approach impractical.

Instead, the bin contents of  $E_{1>}^{\text{in}}$  are estimated in a lattice approximation. In this approximation, 16 Monte Carlo predictions with four values of  $\alpha_s$  and four values of  $\sigma_q$  are generated. These 16 predictions are fit to a quadratic expression of the form

$$N^k(\alpha_s, \sigma_q) = a_{00} + a_{10}\sigma_q + a_{01}\alpha_s + a_{20}\sigma_q^2 + a_{11}\sigma_q\alpha_s + a_{02}\alpha_s^2, \quad (11)$$

where  $N^k(\alpha_s, \sigma_q)$  is the predicted contents of the  $k$ th bin of  $E_{1>}^{\text{in}}$  as a function of  $\alpha_s$  and  $\sigma_q$ . The dependence is found to be nearly linear.

#### 2. Fit of $N^k(\alpha_s, \sigma_q)$ to $E_{1>}^{\text{in}}$

We have previously observed that the high- $E_1$  end of the  $E_{1>}^{\text{in}}$  distribution is less sensitive to variations of the fragmentation parameters. We thus fit bins of  $E_{1>}^{\text{in}}/E_{\text{vis}}$  for  $E_{1>}^{\text{in}}/E_{\text{vis}} \geq 0.2$  where  $E_{1>}^{\text{in}}$  is normalized to  $E_{\text{vis}}$  to minimize the effects of calorimetric fluctuations. These 18 bins are used in a  $\chi^2$  fitting procedure, where  $\chi^2$  is formed from the sum of squared deviations of binned

TABLE I. Best-fit  $\alpha_s$  for (a)  $E_{1>}^{\text{in}}/E_{\text{vis}} > 0.2$  and (b) entire  $E_{1>}^{\text{in}}$  distribution, for string and independent fragmentation. In (a) the first error is statistical and the second error is systematic. In (b) the error is purely statistical. The independent jet models consider gluon fragmentation where  $g \rightarrow q$  or  $g \rightarrow q\bar{q}$ , and energy-momentum conservation according to the Ali or Hoyer schemes, and a case ("No  $E$ - $P$ ") where there is no energy-momentum conservation imposed. Results are given for both the FKSS and GS calculations.

Momentum-conservation scheme	$\alpha_s$ (FKSS)	$\alpha_s$ (GS)	Gluon fragmentation scheme
		(a)	
String	0.167±0.006±0.011	0.133±0.005±0.009	
Ali	0.128±0.007±0.008	0.112±0.008±0.007	} $g \rightarrow q$
Hoyer	0.109±0.007±0.007		
No $E$ - $P$	0.141±0.005±0.009		
Ali	0.125±0.009±0.008		} $g \rightarrow q\bar{q}$
Hoyer	0.109±0.004±0.007		
No $E$ - $P$	0.153±0.007±0.010		
		(b)	
String	0.163±0.003	0.129±0.002	
Ali	0.118±0.005	0.106±0.004	} $g \rightarrow q$
Hoyer	0.090±0.003		
No $E$ - $P$	0.120±0.003		
Ali	0.113±0.005		} $g \rightarrow q\bar{q}$
Hoyer	0.089±0.003		
No $E$ - $P$	0.122±0.003		



data from the Monte Carlo predictions, weighted assuming uncorrelated statistical errors only. Systematic uncertainties are introduced into this procedure by the extent to which a fragmentation model fails to describe fragmentation accurately, and the extent to which the detector simulation fails to model the detector response correctly. We choose not to attempt an estimation of the fragmentation model uncertainties, but instead report  $\alpha_s$  values separately for each model. We can estimate the errors due to inaccuracies in the detector Monte Carlo simulation by considering the difference between  $E_{\perp}^{\text{in}}$  distributions before and after the detector simulation is added. Since the detector simulation adequately reproduces the calorimetric response,<sup>14</sup> this difference represents an upper limit to the errors in the detector modeling. Such a Monte Carlo procedure indicates that the effect of detector resolution is to increase the integrated population of the fitted bins by 6.6%, with a corresponding decrease in the remainder of the normalized distribution. We conservatively assign this entire 6.6% shift to the systematic uncertainty of the detector simulation, which dominates the remaining modeling uncertainties.

### E. Results of the fit

The  $\alpha_s$  values resulting from minimizing the  $\chi^2$  of fits to the high- $E_{\perp}$  end of the  $E_{\perp}^{\text{in}}$  distribution are shown in Table I(a), and those for the entire  $E_{\perp}^{\text{in}}$  distribution are given in Table I(b). The first error in (a) is statistical; the second is systematic. The errors in (b) are purely statistical. The fits were made with string fragmentation and several independent-jet fragmentation models, including the Ali and Hoyer energy-momentum-conservation schemes, and gluon fragmentation according to the  $g \rightarrow q$  and  $g \rightarrow q\bar{q}$  hypotheses. Fits were made separately for the FKSS and GS  $O(\alpha_s^2)$  parton generators. In all cases, the  $\chi^2$  value was no larger than the number of degrees of freedom.

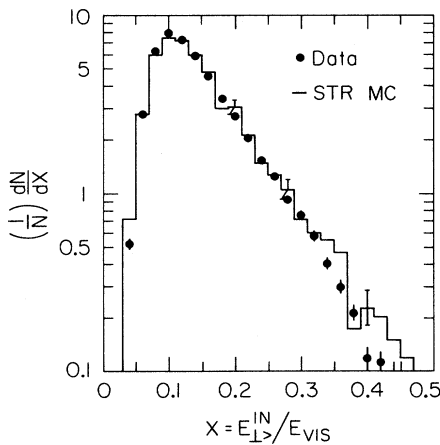


FIG. 11. The string Monte Carlo simulation with partons generated from the GS calculation compared with the data. This Monte Carlo simulation uses the best-fit string values of  $\alpha_s$  of Table I(a). The region  $E_{\perp}^{\text{in}}/E_{\text{vis}} > 0.2$  was used in the fit. Representative statistical error bars for the Monte Carlo are shown.

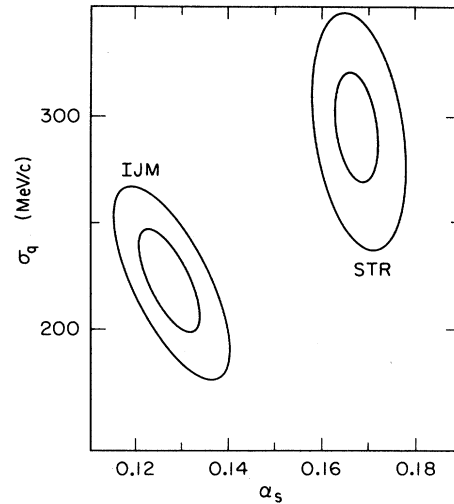


FIG. 12.  $\Delta\chi^2=1$  and  $\Delta\chi^2=2$  contours in  $\alpha_s$  and  $\sigma_q$  fits with independent-jet model (IJM) ( $g \rightarrow q$ , energy-momentum conservation with the Ali scheme) and string fragmentation. There are no values of fragmentation parameters that will allow the independent jet and string models to share a common value of  $\alpha_s$  and still provide reasonable fits to the data.

As a check of the fitting procedure, the best-fit values of  $\alpha_s$  from Table I(a), along with the best-fit values of  $\sigma_q$ , were used as input parameters for a full Monte Carlo simulation of  $E_{\perp}^{\text{in}}$  for comparison with the data. Figure 11 shows a comparison of the data with such a simulation using the string GS value of  $\alpha_s$  from Table I(a). Representative Monte Carlo statistical error bars for the simulation are included in the figure. The fits with the quadratic form for  $N^k(\alpha_s, \sigma_q)$  and the full Monte Carlo simulation both represent the data well.

The best-fit values given in Table I(b) are more sensitive than those in Table I(a) to other fragmentation parameters besides  $\alpha_s$  and  $\sigma_q$ ; no attempt has been made to adjust these other parameters about their nominal value. The fits limited to the high  $E_{\perp}$  end of the  $E_{\perp}^{\text{in}}$  distribution [as given in Table I(a)] are less prone to systematic

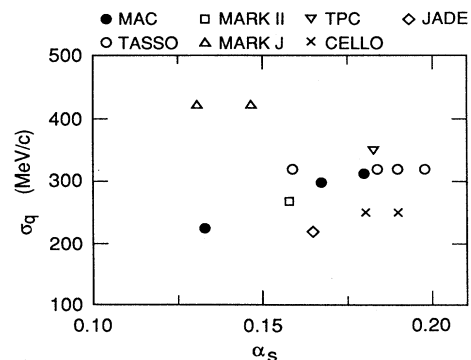


FIG. 13. PEP and PETRA measurements of  $\alpha_s$  and  $\sigma_q$  with the string fragmentation hypothesis, as listed in Table II. Error bars are not shown, but are typically 0.01 in  $\alpha_s$ . Variants of similar TASSO studies are combined into single points.

uncertainties arising from the effects of detector resolution and other fragmentation parameters and hence are the primary result of this study. These values are examined in more detail in the following section.

#### F. Correlations between $\alpha_s$ and $\sigma_q$

In this analysis, we must carefully examine the influence of  $\sigma_q$ . Both  $\alpha_s$  and  $\sigma_q$  contribute to the broadening of the fat jet, so the effect of an inflated  $\sigma_q$  is to mimic a small  $\alpha_s$ . Since the high- $E_\perp$  end of the  $E_{\perp>}^{\text{in}}$  distribution is less sensitive to variations of  $\sigma_q$  than of  $\alpha_s$ , the range of  $\sigma_q$  over which there can be a reasonable fit is quite large. If  $\alpha_s$  and  $\sigma_q$  are correlated, then there might be a common value of  $\alpha_s$  and very different values of  $\sigma_q$  that nonetheless give reasonable fits to the data for independent jet and string models. It is necessary to ensure that the difference in  $\alpha_s$  from fits to different fragmentation models is not an artifact arising from the particular values of the fragmentation parameters used in the fit.

Figure 12 shows that  $\Delta\chi^2=1$  (inner curves) and  $\Delta\chi^2=2$  contours (outer curves) for the fits of  $\alpha_s$  and  $\sigma_q$  to the data for independent jet ( $g \rightarrow q$ , energy-momentum conservation with the Ali scheme) and string fragmentation from a fit to the high- $E_\perp$  end of the  $E_{\perp>}^{\text{in}}$  distribution with the FKSS calculation of the parton distribution. An obvious feature of this figure is a correlation between  $\alpha_s$  and  $\sigma_q$ . Contours for the other independent jet fragmentation schemes show similar qualitative behavior. The string model tends to show less correlation. This might be due to the slightly different role of  $\sigma_q$  in the two models. In independent jet fragmentation,  $\sigma_q$  is the width of the  $p_\perp$  spectrum of the secondary quarks relative to a primary parton direction. In string fragmentation,  $\sigma_q$  is

again the width of the  $p_\perp$  spectrum of the secondary quarks, but here relative to the string direction. In general, the string is boosted with respect to the laboratory frame, and this distinction serves to decouple the string  $\sigma_q$  from the string  $\alpha_s$ . It is important to note, however, that the correlations are not sufficient to allow any overlap between the independent jet and string models in  $(\alpha_s, \sigma_q)$  space. There is no combination of parameters allowing reasonable fits to the data with string and independent jet fragmentation models sharing the same value of  $\alpha_s$ .

#### IV. COMPARISON WITH PREVIOUS RESULTS

There have been a number of  $\alpha_s$  measurements performed at PEP and PETRA with shape, cluster, and energy-energy correlation asymmetry methods. As discussed earlier, the  $O(\alpha_s^2)$  corrections to the QCD matrix elements can be large. We therefore limit comparisons of our results with other measurements to those obtained with  $O(\alpha_s^2)$  QCD matrix elements computed in the modified minimal-subtraction ( $\overline{\text{MS}}$ ) renormalization scheme.<sup>34</sup>

Before detailing other electron-positron measurements of  $\alpha_s$ , we caution that there is no agreement on the values of the soft hadronization parameters to be used and, in general, the fragmentation parameters used by each collaboration in fitting  $\alpha_s$  are unstated. We have seen that it is possible for these parameters (especially  $\sigma_q$ ) to have a substantial effect on the fitted value of  $\alpha_s$ . Figure 13 shows PEP and PETRA values of  $\alpha_s$  and  $\sigma_q$  fitted with string fragmentation.<sup>3,9,35-41</sup> Not all groups reporting  $\alpha_s$  values also report the value of  $\sigma_q$  used. The trend shown in Fig. 13 is for the string value of  $\sigma_q$  to be about 300

TABLE II. PEP and PETRA  $\alpha_s$  values for shape, cluster and EECA. Results of fits to  $\alpha_s$  with string and independent-jet (IJ) fragmentation with  $g \rightarrow q$  and energy-momentum conservation with the Ali scheme are given. Also given are the characteristic  $\sqrt{s}$  and the matrix elements used. The errors shown are the linear sum of the systematic and statistical errors, when the errors are separated in the publication. Otherwise the combined published errors are shown.

Collaboration	Typical $\sqrt{s}$ (GeV)	String $\alpha_s$	IJ $\alpha_s$	Method	Matrix elements
MAC (Ref. 3)	29	0.185±0.013	0.125±0.009	EECA	FKSS
This study	29	0.167±0.017	0.128±0.015	Shape	FKSS
This study	29	0.133±0.014	0.112±0.015	Shape	GS
Mark II (Ref. 35)	29	0.158±0.011	0.10–0.14	EECA	GS
TPC (Ref. 36)	29	0.183±0.010	0.147±0.015	Shape	FKSS
JADE (Ref. 37)	34	0.165±0.02	0.123	EECA	FKSS
TASSO (Ref. 9)	34.6	0.192–0.234	0.145–0.175	Shape	FKSS
		0.174–0.192	0.136–0.147	Cluster	FKSS
		0.190±0.009	0.139±0.009	EECA	FKSS
		0.159±0.012	0.117±0.009	EECA	ERT
Mark J (Ref. 38,39)	36.4	0.131 <sup>+0.010</sup> <sub>-0.013</sub>	0.113 <sup>+0.009</sup> <sub>-0.011</sub>	EECA	ERT
	35	0.147±0.005	0.112±0.005	PTC	ERT
CELLO (Ref. 40)	34	0.18±0.02	0.13±~0.025	Cluster	FKSS
		0.19±0.02	0.15±~0.03	EECA	FKSS
PLUTO (Ref. 41)	34.6	0.145 <sup>+0.004</sup> <sub>-0.004</sub>	0.136 <sup>+0.004</sup> <sub>-0.004</sub>	EECA	ERT

MeV/c or less, with a relatively large spread.

The various PEP and PETRA  $\alpha_s$  measurements<sup>3,9,35-41</sup> from shape, cluster and energy-energy correlation asymmetry are shown in Table II where statistical and systematic errors are combined linearly when separate errors are published. Some collaborations report a value for the QCD scale  $\Lambda_{\overline{MS}}$  so we have converted these values (recognized in Table II by the asymmetric errors in  $\alpha_s$ ) to  $\alpha_s$  for a  $Q^2$  at a characteristic  $\sqrt{s}$  for each to  $O(\alpha_s^2)$ . The  $\alpha_s$  values fitted with the string and independent jet models with  $g \rightarrow q$  and energy-momentum conservation with the Ali scheme are shown, since these two models (or close equivalents) were common to all measurements.

## V. CONCLUSIONS

With the GS calculation, we find at  $\sqrt{s} = 29$  GeV,  $\alpha_s = 0.133 \pm 0.005(\text{stat}) \pm 0.009(\text{syst})$  for string fragmentation, and  $\alpha_s = 0.112 \pm 0.008(\text{stat}) \pm 0.007(\text{syst})$  for a common independent-jet model. The use of partons generated according to the GS calculation results in smaller values of  $\alpha_s$  than FKSS. In the case of string fragmentation, the decrease in  $\alpha_s$  is about 25%. In the case of independent-jet fragmentation with the Ali prescription for energy-momentum conservation, and gluon fragmentation with  $g \rightarrow q$ , the decrease in  $\alpha_s$  is about 15%. Although we present fits of  $\alpha_s$  from various fragmentation models, we do not feel this procedure adequately represents the systematic errors from fragmentation, which remain unknown. In particular, we consider rather dubious the practice of relating the systematic errors of fragmentation to the difference between string fragmentation and the Ali method of independent-jet energy-momentum conservation. Studies indicate that applying a boost to the final-state hadrons mimics string effects,<sup>3,10,37,40</sup> meaning systematic errors estimated in this way are too small. Also, since no calculation of the  $O(\alpha_s^2)$  cross section includes a full treatment of quark masses, their effect remains unknown.

The model dependence between string and independent fragmentation in the FKSS parton calculation observed by many other authors is similarly observed in this study

(see Table II). The FKSS fit of  $\alpha_s$  to independent jet fragmentation with Ali energy-momentum conservation and  $g \rightarrow q$  gluon fragmentation is about 30% smaller than the corresponding FKSS fit to the string-fragmentation hypothesis. Model dependence is also observed when partons from the GS calculation are used, though the model dependence is slightly decreased. In this case, the decrease in the fitted  $\alpha_s$  when string fragmentation is substituted for independent jet fragmentation is about 20%. We conclude that even if the cutoff-dependent terms missing from the FKSS calculation are included, this method results in a minimum model dependence of about 20%.

These  $\alpha_s$  values resulting from the use of the FKSS parton calculation are consistent with previous results shown in Table II. The values of  $\alpha_s$  resulting from the use of the GS calculation are similar to earlier PETRA results from the ERT calculation, even though the experimental methods and perturbative calculations are quite different.

## ACKNOWLEDGMENTS

We thank T. Gottschalk and M. Peskin for helpful discussions. We also wish to thank E. Askeland, N. Erickson, J. Escalera, M. Frankowski, and J. Schroeder for their superb technical assistance. We thank M. Richards for her unfailing support and organizational skills. We would especially like to acknowledge and remember the late C. T. Pulliam, who provided needed engineering skills. R. Coombes was vital and essential for the early years of MAC design, installation, and commissioning, and the subsequent continued successful operation of the detector. This work was supported in part by the U.S. Department of Energy under Contracts Nos. DE-AC02-86ER40253 (University of Colorado), DE-AC03-76SF00515 (SLAC), and DE-AC02-76ER00881 (University of Wisconsin); by the National Science Foundation under Grants Nos. NSF-PHY82-15133 (University of Houston), NSF-PHY82-15413 and NSF-PHY82-15414 (Northeastern University), and NSF-PHY83-08135 (University of Utah); and by the Istituto Nazionale di Fisica Nucleare.

<sup>(a)</sup>Present address: P.O. Box 918-1, Beijing, The People's Republic of China.

<sup>(b)</sup>Present address: Institute of Physics, University of Oslo, P.O. Box 1048, Blindern, Oslo 3, Norway.

<sup>(c)</sup>Present address: CERN, CH-1211 Genève 23, Switzerland.

<sup>(d)</sup>Present address: Department of Physics and Astronomy, Vanderbilt University, Nashville, TN 37235.

<sup>(e)</sup>Present address: Fermilab, Batavia, IL 60510.

<sup>(f)</sup>Present address: Stanford Hospital, Stanford, CA 94305.

<sup>(g)</sup>Present address: Supercollider Central Design Group, LBL 90-4040, Berkeley, CA 94720.

<sup>(h)</sup>Permanent address: CERN, CH-1211 Genève 23, Switzerland.

<sup>(i)</sup>Present address: Enrico Fermi Institute, University of Chicago, Chicago, IL 60637.

<sup>(j)</sup>Present address: Neuron Data, Palo Alto, CA 94301.

<sup>(k)</sup>Present address: Sezione INFN de Pisa, I-56010 San Piero a Grado (PI), Italy.

<sup>(l)</sup>Present address: Laboratorio de Fisica de Altas Energias, Universidad Autónoma de Barcelona, Barcelona, Spain.

<sup>(m)</sup>Present address: Stanford Linear Accelerator Center, Stanford, CA 94309.

<sup>1</sup>TASSO Collaboration, R. Brandelik *et al.*, Phys. Lett. **86B**, 243 (1979).

<sup>2</sup>C. L. Basham, L. S. Brown, S. D. Ellis, and S. T. Love, Phys. Rev. Lett. **23**, 1585 (1978).

<sup>3</sup>MAC Collaboration, E. Fernandez *et al.*, Phys. Rev. D **31**, 2724 (1985). The systematic and statistical errors are added in quadrature.

<sup>4</sup>J. Dorfan, in *Proceedings of the 1983 International Symposium on Lepton and Photon Interactions at High Energies*, Ithaca, New York, 1983, edited by D. G. Cassell and D. L. Kreinick

- (Newman Laboratory for Nuclear Studies, Cornell University, Ithaca, 1983).
- <sup>5</sup>A. De Rújula *et al.*, Nucl. Phys. **B138**, 387 (1978).
- <sup>6</sup>A. Ali and F. Barreiro, Nucl. Phys. **B236**, 269 (1984).
- <sup>7</sup>S. D. Ellis, Phys. Lett. **117B**, 333 (1982).
- <sup>8</sup>H. Georgi and M. Machacek, Phys. Rev. Lett. **39**, 1237 (1977).
- <sup>9</sup>TASSO Collaboration, M. Althoff *et al.*, Z. Phys. C **26**, 157 (1984). The systematic and statistical errors are added in quadrature.
- <sup>10</sup>T. Sjöstrand, Z. Phys. C **26**, 93 (1984).
- <sup>11</sup>Z. Kunszt, Phys. Lett. **99B**, 429 (1981); **107B**, 123 (1981).
- <sup>12</sup>T. D. Gottschalk and M. P. Shatz, California Institute of Technology Report No. CALT-68-1172, 1985 (unpublished). This is not to be confused with the QCD shower model of T. D. Gottschalk and D. Morris, California Institute of Technology Report No. CALT-68-1365, 1986 (unpublished).
- <sup>13</sup>W. T. Ford, in *Proceedings of the International Conference on Instrumentation for Colliding Beam Physics*, Stanford, California, 1982, edited by W. W. Ash (SLAC Report No. 250, Stanford, 1982), p. 174.
- <sup>14</sup>MAC Collaboration, E. Fernandez *et al.*, Phys. Rev. D **31**, 1537 (1985).
- <sup>15</sup>E. Cisneros *et al.*, IEEE Trans. Nucl. Sci. **NS-24**, 413 (1977).
- <sup>16</sup>M. Breidenbach *et al.*, IEEE Trans. Nucl. Sci. **NS-25**, 706 (1978).
- <sup>17</sup>R. Anderson *et al.*, IEEE Trans. Nucl. Sci. **NS-25**, 340 (1978).
- <sup>18</sup>E. Farhi, Phys. Rev. Lett. **39**, 1587 (1977).
- <sup>19</sup>R. K. Ellis, D. A. Ross, and A. E. Terrano, Nucl. Phys. **B178**, 421 (1981); K. Gaemers and J. Vermaseren, Z. Phys. C **7**, 81 (1980); A. Ali *et al.*, Nucl. Phys. **B167**, 454 (1980).
- <sup>20</sup>M. Dine and J. Sapirstein, Phys. Rev. **43**, 668 (1979); V. G. Chetyrkin, A. L. Kataev, and F. V. Tkachev, Phys. Lett. **85B**, 277 (1979); W. Celmaster and R. J. Gonsalves, Phys. Rev. Lett. **44**, 560 (1980).
- <sup>21</sup>K. Fabricius, G. Kramer, G. Schierholz, and I. Schmitt, Phys. Lett. **97B**, 431 (1980); Z. Phys. C **11**, 315 (1981); F. Gutbrod, G. Kramer, and G. Schierholz, *ibid.* **21**, 235 (1984).
- <sup>22</sup>T. D. Gottschalk and M. P. Shatz, Phys. Lett. **150B**, 451 (1985).
- <sup>23</sup>We use a modified version of the Lund JETSET version 5.2 FORTRAN code (see Ref. 28) to simulate fragmentation. The event simulation is detailed in L. J. Rosenberg, Ph.D. thesis, SLAC Report No. 289, 1985.
- <sup>24</sup>Mark J Collaboration, B. Adeva *et al.*, Phys. Rev. Lett. **50**, 2051 (1983).
- <sup>25</sup>The predictions of the ERT calculation are those of R. Zhu, Ph.D. thesis, Massachusetts Institute of Technology, Department of Physics, 1983.
- <sup>26</sup>There are two common methods of implementing resolution cuts: direct dressing and partial fraction dressing. The two schemes are discussed in Ref. 22. The GS calculation uses partial fraction dressing. The ERT calculation as implemented in Monte Carlo calculations uses several sequential cuts.
- <sup>27</sup>B. L. Ioffe, Phys. Lett. **78B**, 277 (1978).
- <sup>28</sup>T. Sjöstrand, Comput. Phys. Commun. **28**, 229 (1983).
- <sup>29</sup>W. Hofmann, *Jets of Hadrons* (Springer, Berlin, 1981), pp. 25–45.
- <sup>30</sup>C. Peterson *et al.*, Phys. Rev. D **27**, 105 (1983).
- <sup>31</sup>J. Izen, in *Multiparticle Dynamics 1984*, proceedings of the XVth International Symposium, Lund, Sweden, 1984, edited by G. Gustafson and C. Peterson (World Scientific, Singapore, 1984), p. 727.
- <sup>32</sup>R. Field and R. P. Feynman, Nucl. Phys. **B136**, 1 (1978).
- <sup>33</sup>R. Schwitters in *Proceedings of the International Symposium on Lepton and Photon Interactions at High Energies*, Stanford, California, 1975, edited by W. T. Kirk (SLAC, Stanford, 1976).
- <sup>34</sup>W. A. Bardeen, A. J. Buras, D. W. Duke, and T. Muta, Phys. Rev. D **18**, 3998 (1978).
- <sup>35</sup>Mark II Collaboration, D. R. Wood *et al.*, Phys. Rev. D **37**, 3091 (1988).
- <sup>36</sup>TPC Collaboration, H. Aihara *et al.*, Z. Phys. C **28**, 31 (1985). The systematic and statistical errors are added in quadrature. This is a study of fragmentation models, not primarily a study of  $\alpha_s$ .
- <sup>37</sup>JADE Collaboration, W. Bartel *et al.*, Z. Phys. C **25**, 231 (1984). They report an  $\alpha_s$  value from a direct fit to QCD predictions in B. Naroska, Phys. Rep. **148**, 67 (1987).
- <sup>38</sup>Mark J Collaboration, B. Adeva *et al.*, Phys. Rev. Lett. **54**, 1750 (1985).
- <sup>39</sup>Mark J. Collaboration, B. Adeva *et al.*, Phys. Lett. **B 180**, 181 (1986). The table lists only statistical errors. They also report a combined (string and independent-jet)  $\alpha_s$  value from data taken over a broad energy range. Their fits were made to the planar triple energy correlation, an analog of the energy-energy correlation.
- <sup>40</sup>CELLO Collaboration, H. Behrend *et al.*, Phys. Lett. **138B**, 311 (1984). The cluster and EECA string values show statistical errors only. They also report an  $\alpha_s$  value based on  $R$ -value measurements in H. Behrend *et al.*, Phys. Lett. **B 183**, 400 (1987).
- <sup>41</sup>PLUTO Collaboration, Ch. Berger *et al.*, Z. Phys. C **28**, 365 (1985). This is from a fit to the entire EECA distribution. The errors are presumed purely statistical. They also fit  $\alpha_s$  directly to perturbative QCD predictions.